

## Molecular Dynamics Simulation of Site-Directed Spin Labeling: Experimental Validation in Muscle Fibers

Leslie E. W. LaConte, Vincent Voelz, Wendy Nelson, Michael Enz, and David D. Thomas

Biochemistry, Molecular Biology, and Biophysics Department, University of Minnesota, Minneapolis, Minnesota 55455 USA

**ABSTRACT** We have developed a computational molecular dynamics technique to simulate the motions of spin labels bound to the regulatory domain of scallop myosin. These calculations were then directly compared with site-directed spin labeling experimental results obtained by preparing seven single-cysteine mutants of the smooth muscle (chicken gizzard) myosin regulatory light chain and performing electron paramagnetic resonance experiments on these spin-labeled regulatory light chains in functional scallop muscle fibers. We determined molecular dynamics simulation conditions necessary for obtaining a convergent orientational trajectory of the spin label, and from these trajectories we then calculated correlation times, orientational distributions, and order parameters. Simulated order parameters closely match those determined experimentally, validating our molecular dynamics modeling technique, and demonstrating our ability to predict preferred sites for labeling by computer simulation. In several cases, more than one rotational mode was observed within the 14-ns trajectory, suggesting that the spin label samples several local energy minima. This study uses molecular dynamics simulations of an experimental system to explore and enhance the site-directed spin labeling technique.

### INTRODUCTION

Site-directed spin labeling (SDSL) is a powerful technique to probe protein dynamics and conformation (Hubbell and Altenbach, 1994; Hubbell et al., 2000). Using site-directed cysteine mutagenesis, spin labels are attached throughout a protein, one site per sample, and electron paramagnetic resonance (EPR) spectra are used to measure spin label rotational mobility and accessibility and to interpret this data in terms of protein secondary and tertiary structure. There is a large body of evidence to show that the restriction of nanosecond dynamic disorder exhibited by a spin label attached to a protein is a direct reflection of the local structure and dynamics of the protein, due to nearby residues within the protein or to contacts made with other molecules. Indeed, the size of a binding pocket can be measured by probe mobility as the steric effect of differently sized substituents (Columbus et al., 2001).

When attached to a specific protein residue, probe restriction should be well modeled by a molecular dynamics (MD) simulation reflecting the restrictions imposed by neighboring protein atoms. EPR spectroscopy has the right spectral resolution and time scale to test the validity of MD simulations. The extent of narrowing of the nitroxide EPR spectrum is optimally sensitive to the amplitude (measured by the order parameter) of nanosecond and subnanosecond rotational motions. It should be possible to calculate the order parameter accurately from an MD simulation, provided that the probe orientational trajectory reaches equilibrium within a few nanoseconds.

Steinhoff and Hubbell have shown that MD trajectories of a nitroxide spin label attached to a tripeptide with fixed  $C_{\alpha}$ s generally reach equilibrium within a few nanoseconds and yield EPR simulations that show good qualitative agreement with whole-protein EPR experiments in which structurally homologous residues were labeled (Steinhoff and Hubbell, 1996). In the present study we apply a similar approach to MD simulations based directly on a protein crystal structure.

### Spin-labeled muscle fibers as a model system

Muscle fibers provide an excellent system in which to test both the SDSL technique and the accuracy of modeling using MD. When spin labels are rigidly and stereospecifically bound to sites within the muscle fiber, experimentalists can take advantage of the highly ordered, oriented system to study rigid-body motion of protein structures (Thomas and Cooke, 1980). In the case of an unoriented sample, measurements of probe mobility can directly reflect local conformational changes within muscle proteins (Ostap et al., 1993). The regulatory light chain (RLC) of myosin can be easily exchanged in a muscle fiber, offering the opportunity to use molecular biology to engineer specific spin-labeling sites to investigate local structure or global movement (Baker et al., 1998; Roopnarine et al., 1998).

EPR spectroscopy of spin-labeled myosin has demonstrated that the regulatory domain undergoes a  $\sim 36^\circ$  rotation upon muscle contraction, acting as a lever arm to produce mechanical force. This result was found by spin labeling the single native cysteine residue (Cys-108) of the chicken gizzard RLC incorporated into myosin in scallop muscle fibers (Baker et al., 1998). The spin label 3-(5-fluoro-2,4-dinitroanilino)-2,2,5,5-tetramethyl-1-pyrrolidinyl-1-oxyl (FDNASL) binds specifically and rigidly to Cys-108, resulting in a probe that is sensitive to the orientation

*Submitted January 27, 2002, and accepted for publication May 13, 2002.*

Leslie E. W. LaConte and Vincent Voelz contributed equally to this work.

Address reprint requests to David D. Thomas, University of Minnesota, Biochemistry, Molecular Biology and Biophysics Department, 321 Church Street SE, 6-155 Jackson Hall, Minneapolis, Minnesota 55455. Tel.: 612-625-0957; Fax: 612-624-0632; E-mail: ddt@ddt.biochem.umn.edu.

© 2002 by the Biophysical Society

0006-3495/02/10/1854/13 \$2.00

of the regulatory domain relative to the muscle fiber. We sought to complement this SDSL study by systematically making several site-directed single-cysteine mutants on the RLC, attaching FDNASL, and measuring their EPR spectra in an oriented muscle fiber, thus potentially mapping out orientational conformations of the RLC. However, it remained a significant challenge to choose labeling sites that would yield restricted probes. There is a low probability that any one Cys mutant will possess both functionality and a rigidly bound, oriented probe, so identifying suitable residues by trial-and-error mutagenesis, expression, and purification of individual RLC mutants is very time consuming.

We reasoned that a MD simulation of a spin-labeled protein might shorten this process by predicting which labeling sites will produce the desired level of orientation and mobility. By performing these simulations on an experimentally accessible system, the present study offers a direct test of the MD calculation, representing a significant advance over previous studies of spin label dynamics (Steinhoff and Hubbell, 1996). Order parameters of specific spin-labeled mutants can be predicted and then compared directly with order parameters measured experimentally, verifying both the SDSL and MD techniques.

A detailed MD simulation of spin labels also presents us with ways to supplement EPR spectral measurements to resolve otherwise ambiguous conclusions. Absolute orientation of probe trajectories with respect to a known reference frame can give information about the conformations of the proteins to which they are attached. It is also possible to simulate EPR spectra directly from probe trajectories and compare these with measured spectra (Freed, 1976; Robinson et al., 1992; Steinhoff and Hubbell, 1996). This presents the possibility of resolving ambiguous spectral shapes with unprecedented detail, e.g., by separating the competing effects of orientational disorder and fast-motional EPR tensor averaging. Furthermore, by performing long MD simulations at many different labeling sites, we can begin to get a picture of the general properties of attached spin probes and what factors are important in determining their dynamic behavior.

In the present paper, we first describe our computational methods and then examine in detail the dynamic behavior of a series of spin-labeled myosin RLC mutants over long MD simulations (14 ns). MD simulation is shown to accurately predict observed order parameters as measured by EPR spectroscopy, providing an excellent way to predict the usefulness of proposed site-directed mutants.

## MATERIALS AND METHODS

### Experimental system

#### Sample preparation

RLC was purified from fresh chicken gizzard myosin (Persechini and Hartshorne, 1983), then spin-labeled with FDNASL as described previ-

ously (Baker et al., 1998). Muscle fiber bundles were prepared from *Placopecten magellanicus* (sea scallop) adductor muscle, and the native RLC was exchanged for the labeled chicken gizzard RLC, as described previously (Brust-Mascher et al., 1999). These fiber bundle samples were placed in capillaries for EPR spectral acquisition. Minced fibers were prepared by cutting labeled fibers into fragments with dissection scissors and were then flowed into capillaries and trapped with glass wool or placed in the well of a flat cell for spectral acquisition.

### RLC mutant expression and purification

Chicken gizzard RLC mutants were prepared using a null cysteine (C108A) cDNA construct, kindly provided by Dr. Renne Lu from the Boston Biomedical Research Institute. This cDNA was ligated into the pet3a expression system (Novagen, Madison, WI) between the sites NEI and *Eco*RI. Using the QuikChange Mutagenesis system (Stratagene, La Jolla, CA), single cysteines were mutated at desired positions in the RLC. The pet3a-RLC with the desired mutation was then cotransformed with the pLys plasmid (Novagen) into the *Escherichia coli* expression strain, JM109DE3. The pLys plasmid encodes for T7 lysozyme, which shuts down basal transcription and stabilizes the pet3a-RLC plasmid. For each mutant, a 10-mL overnight culture was used to inoculate a large 1-L culture. The cells were incubated, shaking at 37°C until an optical density of 0.6 was reached, and then induced with IPTG (isopropyl 1-thio- $\beta$ -D-galactopyranoside). The culture was incubated at 37°C for another 3 h, and the cells were harvested by centrifugation at  $5000 \times g$  for 10 min. The cells were resuspended in 50 mL of 25 mM Tris-HCl, pH 8.0, 5 mM EDTA, 50 mM glucose, 1 mM phenylmethylsulfonyl fluoride, and 0.2 mg of lysozyme. The suspension was incubated on ice for 1 h and subjected to one cycle of freeze/thaw using an isopropanol/dry ice bath. The cells were then incubated with 10 mM MgCl<sub>2</sub> and 5  $\mu$ g/mL DNase for 1 h. Triton was added to 0.1%, and the cells were centrifuged at  $15,000 \times g$  for 15 min. Two more washes with the above buffer and 0.1% Triton were carried out, and one final wash was done without Triton. The pellet was dissolved in 10 mL of 7 M urea, 30 mM Tris-HCl, pH 7.5, 50 mM NaCl, and 1 mM dithiothreitol and centrifuged at  $100,000 \times g$  for 30 min. A DE-52 (Whatman, Clifton, NJ) anion exchange column was equilibrated with 4 M urea, 30 mM Tris-HCl, pH 7.5, 50 mM NaCl, and 1 mM dithiothreitol. The supernatant was applied to the column, and a linear gradient from 0.05 to 0.3 M NaCl was used to elute the RLC. The fractions containing RLC were pooled and dialyzed against 5 mM ammonium bicarbonate and then lyophilized.

### EPR spectroscopy

X-band EPR spectra were acquired on a Bruker ESP 300 spectrometer or a Bruker EleXsys 500 spectrometer (Bruker Instruments, Billerica, MA). Spectra of oriented muscle fibers and randomly oriented minced fibers were acquired as described previously. Spectra were obtained in rigor buffer (20 mM MOPS, 5 mM MgCl<sub>2</sub>, 1 mM EGTA, and 0.1 mM NaN<sub>3</sub>, pH 7).

## Molecular dynamics model

### Base structure and molecular model

Because a high-resolution crystal structure of chicken gizzard regulatory domain is unavailable, the known sequence (Maita et al., 1984) was homology-modeled onto the 2.8-Å resolution crystal structure of scallop myosin regulatory domain (Xie et al., 1994, PDB structure 1scm) using the homology module of *InsightII/Biosym*. Sequence homology between the scallop regulatory light chain (Maita et al., 1984) and chicken gizzard regulatory light chain (Maita et al., 1981) was determined by BLAST to be 47% identical and 70% similar. The final molecular model consists of 5597

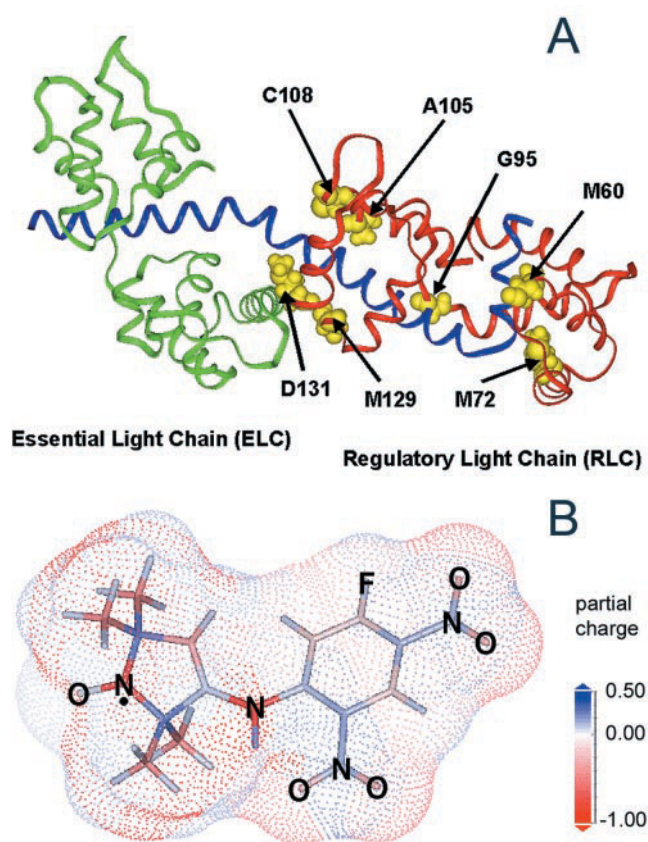


FIGURE 1 (A) Models of several experimental mutants produced by site-directed mutagenesis were constructed in InsightII: C108 (wild type), A105C, M129C, and D131C. Other “predicted” mutants were also constructed: M60C, M72C, and G95C. (B) Spin label FDNASL and its partial charges.

atoms: 359 residues including a section of the heavy chain (M773-L837), the ELC (L3-P154), the RLC (L12-E153), and two  $\text{Ca}^{2+}$  ions. Disordered residues not in the crystal structure were not included in the model.

### Attaching the probe to the structure

To model a particular spin-labeled mutant, the native residue was replaced by cysteine, the native cysteine replaced by alanine, and the probe molecule covalently attached to its associated sulfur atom. In each case, the mutated residue was appended to the C terminus of the RLC, which conserves molecular mass across all the mutants so their energies can be compared. Models of the wild-type structure (C108) and several mutants produced by site-directed mutagenesis were constructed: A105C, M129C, and D131C. Other “predicted” mutants, G65C, M72C, and G95C were first constructed computationally and later expressed experimentally (Fig. 1 A).

### Energy minimization and MD performed locally around the probe

Energy minimization and MD were calculated using the Discover3 engine from InsightII/Biosym. We restricted our attention to local minimization and dynamics around the probe; this is justified because experimental mutants are completely functional and we expect the regulatory domain to be minimally perturbed by the presence of the probe. Due to the truncated

nature of the model, both from the missing residues in the crystal structure and its detachment from the larger myosin S1 complex, it is prudent to consider only the local dynamics of the probe. As documented in Results and Discussion, we determined that a simulation including atoms within a 20-Å radius around the probe gave accurate results, after examining convergence criteria from simulations of radii ranging from 14 to 24 Å.

**Force field parameters.** The CVFF force field (Dauber-Osguthorpe et al., 1988) was used for energy minimization and dynamics. Standard atomic potentials for peptides were assigned to the homology-modeled structure after correcting new double bonds. Unique partial charges for the probe were calculated with the program MOPAC, using Mulliken partial charges for FDNASL (Fig. 1 B) using the AM1 Hamiltonian (Dewar et al., 1985). To account for the unusual electronic structure in the nitroxide group, the nitrogen atom was assigned parameters for a partial double bond, preserving the planar orientation of the oxygen. All simulations were calculated in vacuo with no counter ions and no ionized residues.

**Energy minimization.** For each structure, atoms within 20 Å of the probe were energy-minimized in vacuo using the conjugate gradient method to within  $0.01 \text{ kcal}\cdot\text{mol}^{-1}\cdot\text{\AA}^{-1}$ . The same method was then applied to the entire molecule for 50,000 iterations, yielding a maximum derivative of  $\sim 1.5 \text{ kcal}\cdot\text{mol}^{-1}\cdot\text{\AA}^{-1}$  for the entire protein. This accounted for larger-scale relaxations upon perturbation by a probe.

**Molecular dynamics.** MD calculations were performed within a subset of allowed motion, defined to be all atoms within 20 Å from the nitroxide N in FDNASL. If a  $\text{Ca}^{2+}$  ion was within this distance, its position was fixed throughout the simulation. Atoms more than 45 Å from the probe were ignored, whereas atoms between 20 and 45 Å were included in the simulation but fixed in position. Trajectory points were calculated in 3-fs time steps using the Velocity Verlet method. The RATTLE algorithm was used to constrain hydrogen bond lengths to a tolerance of  $10^{-5}$ . Using this, the simulation was stable with a 3-fs time step. The trajectory of the entire simulation was written to file every 20 ps. Nonbonded force field terms were calculated using the cell multipole method with a 10-Å cutoff, 1.0-Å update width, and fixed intrinsic dielectric constant  $\epsilon = 1.0$ . The thermodynamic ensemble was (constant number, volume, and temperature),  $T = 298 \text{ K} \pm 10 \text{ K}$  tolerance by velocity scaling. All simulations were run on a network of queued SGI Origin 200 computers, on multiple 195 MHz R10000 processors.

In most cases, 14-ns trajectories were assembled from shorter 1, 2, and 4 ns trajectories, each continued from a “restart” file. At these “restart” points, the simulation was resumed with the previous atom positions from the last time step, but with atom velocities reassigned randomly from a Boltzmann distribution at 300 K. This provided a convenient way to test the stability of the simulation with respect to perturbation.

The nitroxide EPR spectrum is determined almost entirely by the time-dependence of the angles  $\theta$  and  $\phi$  that define the orientation of the applied magnetic field  $H$  with respect to the principal axis system of the nitroxide group, as indicated in Fig. 2. Therefore, to enable calculation of EPR parameters from the trajectory, coordinates of the spin probe N-O vector and the probe’s p-orbital z-axis, defined as the cross-product of the  $\text{C}_2\text{-N}$  and  $\text{C}_5\text{-N}$  vectors (Fig. 2), were written to file at every time step.

### Alignment of light chain domain

To determine the orientation of the spin label relative to the muscle fiber (actin filament) axis (which is aligned with the magnetic field  $H$  in our experiments), we started from the structure of an actin filament decorated with chicken skeletal S1 (Mendelson and Morris, 1997), and aligned our MD model of the spin-labeled regulatory domain onto the structure using the 19 residues in the heavy chain closest to the catalytic domain, 782 to 800. Although the length of the heavy chain in our MD model extends beyond residue 800, we did not use those residues for alignment, because the structures of the regulatory domains for skeletal and scallop muscle appear to diverge beyond that point (Houdusse and Cohen, 1996).



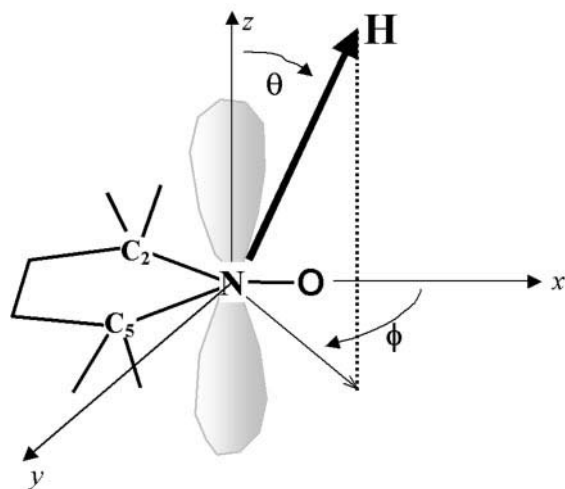


FIGURE 2 Geometry of the spin probe.  $H$  is the laboratory-frame magnetic field, oriented with spherical angles  $\theta$ ,  $\phi$  with the nitroxide  $z$  axis.

### Calculation of order parameters from probe trajectories

To compare quantitatively the results of the MD simulation with experimental EPR data, we calculated the spin label order parameter

$$S = 1.5\langle \cos^2 \beta \rangle - 0.5, \quad (1)$$

in which  $\langle \cos^2 \beta \rangle = \int \cos^2 \beta \rho(\beta) \sin \beta d\beta$ , directly from the MD trajectory, in which  $\beta$  is the angular deviation from the mode of the orientational distribution of the  $z$  axis of the nitroxide (Fig. 3). This order parameter determines the EPR spectrum for rapid restricted rotational diffusion in a randomly oriented sample, as discussed below. The distribution  $\rho(\beta)$  is calculated by first determining the distribution of  $\theta$  values (Fig. 2), then defining  $\beta = 0$  at the mode of this distribution. A Windows C++ program called Dynamics was used to analyze and display trajectory data. The program also calculates the probe's angular distribution with respect to the muscle fiber axis, which corresponds to the distribution of the angles  $\theta$  and  $\phi$  in Fig. 2 in the case of a muscle fiber oriented parallel to the applied field.

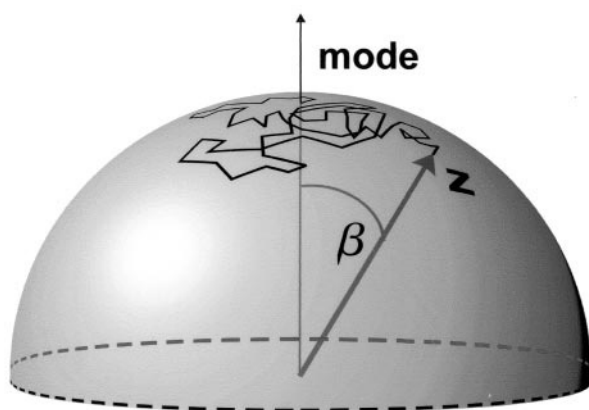


FIGURE 3 Relationship between orientational trajectory  $\beta(t)$  and order parameter  $S$ .  $\beta$  is the angle between the  $z$  axis of the spin label and the mode vector, which defines the center of the orientational distribution  $\rho(\beta)$ .  $S$  is calculated from  $\rho(\beta)$  as described in Eq. 1.

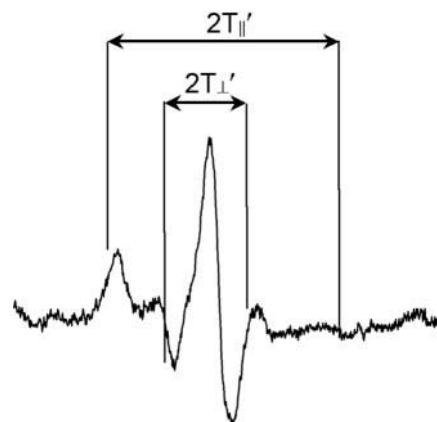


FIGURE 4 Spectral line-splittings are used to calculate order parameter ( $S$ ) from an EPR spectrum according to Eq. 2 (spectrum example shown is of spin-labeled M129C in randomly oriented fibers).

Experimental order parameters were calculated from the EPR spectra of spin-labeled proteins that were randomly oriented (Fig. 4). For most practical purposes, the apparent order parameter  $S$  can be calculated by the ratio of the measured anisotropic hyperfine splittings ( $T_{\parallel}' - T_{\perp}'$ ) to the maximum possible tensor values ( $T_{\parallel} - T_{\perp}$ ) (Gaffney, 1976; Squier and Thomas, 1989):

$$S = \frac{T_{\parallel}' - T_{\perp}'}{T_{\parallel} - T_{\perp}} \quad (2)$$

Errors stemming from this approximate expression are small, negligible except in the limiting case of high disorder ( $S < 0.1$ ).

### Autocorrelation of probe trajectories

We define the autocorrelation of a probe trajectory of length  $T$  to be

$$G(\tau) = \frac{1}{T} \int_{t_0}^{t_0+\tau} \cos \beta(t) \cos \beta(t + \tau) dt \quad (3)$$

in which  $\beta(t)$  is the angle of the  $z$  axis of the nitroxide with the mode of the trajectory. We take the autocorrelation over the cosine of the mode angle because of the useful quantities  $G(0) = \langle \cos^2 \beta \rangle$  and  $\lim_{\tau \rightarrow \infty} G(\tau) = \langle \cos \beta \rangle^2$ , from which order parameter can be calculated (Eq. 1). The rotational correlation time is defined from the best fit to  $G(\tau) = G(0)\exp(-\tau/\tau_c)$  over a specified time window.

### Spin label and side-chain radial distributions, RMS, and diffusion constants

To understand the relationship between the calculated order parameter and the spin label's environment, we analyzed the distances from the spin label and adjacent residues across the MD trajectory. For groups of atoms  $a$  and  $b$ , INSIGHT calculates the radial distribution function  $\rho_{a-b}(r)$ , the proba-

bility that atoms from groups  $a$  and  $b$  are separated by distance  $r$ . Then the rms distance  $r_{\text{rms}}$  is calculated from

$$r_{\text{rms}} = \left( \int_0^\infty r^2 \rho_{a-b}(r) dr \right)^{1/2} = \sqrt{\langle r^2 \rangle} \quad (4)$$

and standard deviations  $\sigma$  by

$$\sigma^2 = \langle r^2 \rangle - \left( \int_0^\infty r \rho_{a-b}(r) dr \right)^2 = \langle r^2 \rangle - \langle r \rangle^2 \quad (5)$$

The relative diffusion coefficient of two atom groups is then calculated as

$$D = \langle r^2(t) \rangle / 6t \quad (6)$$

for long times  $t$  (Tinoco et al., 1985).

The values of  $r_{\text{rms}}$  and  $D$ , between a residue and a spin label segment, were calculated across 698 time points along a 14-ns trajectory (every 20 ps). Atom groups for nearby residues were defined as all atoms in the side chain including the  $C_\alpha$ . Distances were calculated from each residue to the entire spin label and also to each of its two major segments.

## RESULTS AND DISCUSSION

### Convergence and consistency of MD trajectories

We used C108-FDNASL as a test case to demonstrate that our simulation produces convergent, self-consistent dynamics trajectories that are insensitive to velocity perturbations (Allen and Tildesley, 1987). We also measured the sensitivity of the simulation to starting conformer.

Most trajectories converged within 1 ns with potential energy and rms differences remaining stable over the entire 14-ns trajectory (Fig. 5), giving equivalent results in independent runs. The potential energy (Fig. 5 *A*) and RMS differences from the starting structure (Fig. 5 *B*) converged within 500 ps. With the exception of A105C-FDNASL (discussed below), the trajectories were insensitive to velocity perturbations (Fig. 5 *C*).

### Determining an appropriate simulation subset of allowed motion

To determine the appropriate size of the movable subset of atoms, we calculated 14-ns trajectories in which the movable subset had radii ranging from 14 to 24 Å (Fig. 6). All dynamics trajectories had nearly identical average conformations. The principal correlation time, determined by fitting the autocorrelation function to a single exponential, was less than 50 ps in each case. This rapid convergence of the orientational distribution justifies the calculation of an order parameter  $S$  (Eq. 1) that characterizes the amplitude of subnanosecond probe rotational motion. The order parameter decreased significantly with increasing radius, suggesting that artifactual motional constraints were significant at short radii but converged for radii of 18 Å and greater (see Fig. 8). Therefore, we used a radius of 20 Å in all subse-

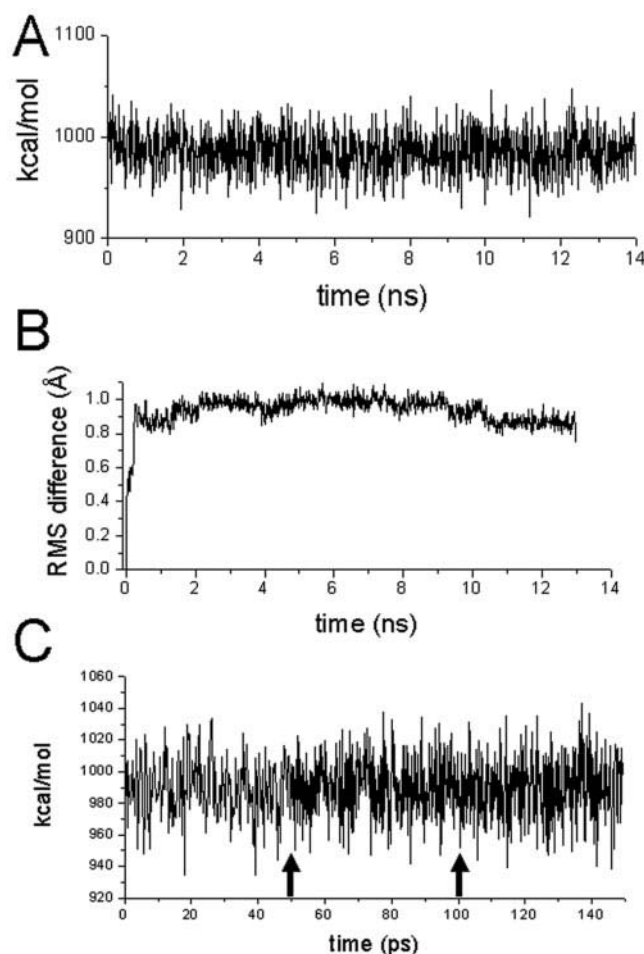


FIGURE 5 Typical convergence of MD trajectories, shown here for the myosin regulatory domain spin-labeled at C108. (*A*) Total potential energy. (*B*) The RMS difference in atom positions, including all movable atoms, relative to the starting conformation. (*C*) First 150 ps of an MD trajectory in which velocity perturbations were applied every 50 ps (as marked by arrows).

quent simulations. These results highlight the importance of examining the effects of simulation constraints to avoid significant artifacts.

### Convergence sensitivity to starting conformation

C108-FDNASL was used as a test case to examine the sensitivity of convergence to the starting conformation. When the initial position of the spin label was manually repositioned in the minimized structure to five different conformations, all trajectories converged within 500 ps to essentially identical structures and energies. To examine convergence sensitivity with more distant starting conformations, a 200-ps trajectory of C108-FDNASL at 600-K was simulated, and eight low-potential energy conformers were chosen from approximately every 50 ps in the trajectory. This created a series of conformations that were in

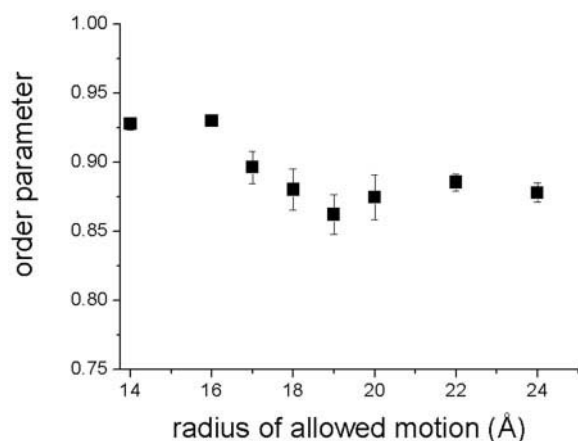


FIGURE 6 Order parameters of C108-FDNASL trajectories shown as a function of the radius of allowed motion. Points plotted are mean  $\pm$  SE of order parameter across 1-ns trajectory segments.

creasingly farther away on the energy landscape from the original minimized starting structure. These conformations were then used as starting structures for subsequent dynamics for 6 ns at 300 K. The trajectories uniformly converge over the first 1 ns to single-mode dynamics about several local minima stable over the 6-ns simulation. The three lowest-energy trajectories that were computed—each with an RMS difference from the starting structure of less than 1.3 Å—reproduced the trajectory originally determined by our minimization and dynamics methods, whereas the higher-energy trajectories did not. Besides having higher potential energies, the trajectories about more distant local minima were distinguished by their lower calculated order parameters across the last 2 ns of the trajectory (Fig. 7) and distortion of the peptide backbone conformation incongruent with the crystal structure. No lower-energy minima were found. We conclude that C108-FDNASL has a well-defined energy minimum determined by our methods and that start-

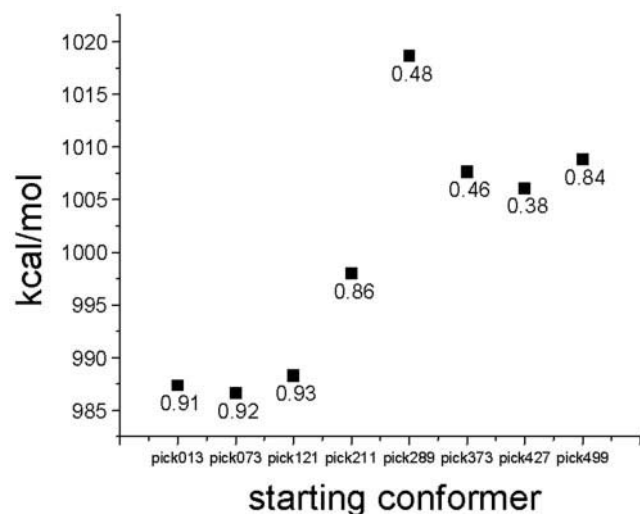


FIGURE 7 Convergence sensitivity to starting conformer. The average potential energy of each local minimal conformer is plotted, and its respective order parameter is shown below each data point.

ing conformations different by more than an RMS distance of  $\sim 1.3$  Å from the average structure will not produce the correct dynamics within the length of our simulation.

### Trajectories of FDNASL-RLC mutants

Shown in Fig. 8, for each spin-labeled site, is the experimentally determined EPR spectrum, the simulated 14-ns MD trajectory, and the angular distribution of the probe.

### Commonalities among the trajectories

The trajectories (Fig. 8, center) and their corresponding distribution functions (Fig. 8, right) reveal the number of local orientational states and the extent of rotational disorder about each state. In several cases, the probe orientation  $\beta$  shows evidence of jumping between discrete orientational states, whereas the energy of the entire system shows a single well-defined energy minimum. Inspection of the structures reveals a simple explanation: the primary source of motion among the reorientational states is the rotation of the relatively rigid five-membered pyrrolidiny ring about its proximal amine bond. This has been suggested previously for other spin labels, based on MD simulations (Steinhoff and Hubbell, 1996) and experiments (Columbus et al., 2001; Langen et al., 2000). Whereas internal steric hindrance in the spin label favors a *trans* conformer of the pyrrolidiny ring with respect to the amine group (as shown in Fig. 1 B), thermal motion is apparently enough to overcome this activation barrier in favorable cases.

We will now discuss briefly the distinguishing characteristics of each spin-labeled site.

#### C108

EPR experiments have shown that the spin label attached to this site is quite restricted in its rotational mobility with respect to the protein (Baker et al., 1998) with an order parameter of 0.82. The simulated MD trajectory displays similar restricted probe dynamics, approximating a single Gaussian mode (Fig. 8). Fourteen nanoseconds of MD with velocity perturbation failed to produce dynamics about any other local minima. Inspection of the structure shows that the probe rests in a pocket between the two light chains and is stabilized by steric interactions with two nearby leucines on the heavy chain and possible van der Waals interactions between the phenyl ring of FDNASL and nearby F109.

#### D131C

The spin label attached to C131 resides in a relatively exposed pocket between the two light chains. As a result, long bimodal fluctuations of the pyrrolidiny ring are seen on the order of  $\sim 1$  ns. Approximately 9 ns into the trajectory, nearby R813 on the heavy chain assumes a new rotameric conformation, causing a small change in steric boundaries, and a slight change in the conformation of the

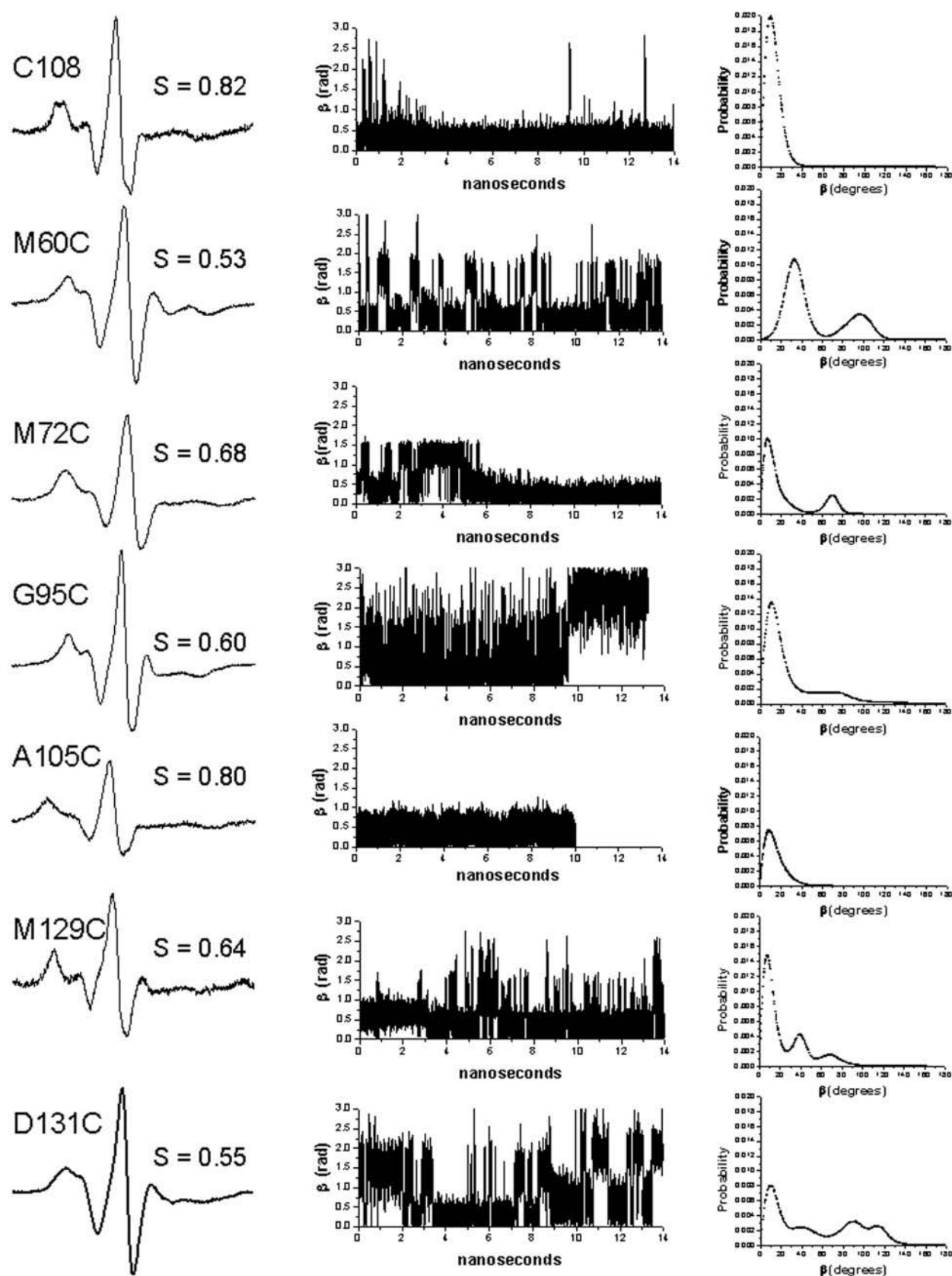


FIGURE 8 EPR spectra and simulated spin probe trajectories over 14 ns for randomly oriented FDNASL-labeled regulatory domains for seven different sites. (Left) Experimental EPR spectrum and order parameter  $S$ . (Middle) Orientational trajectory of the spin label in which the angle  $\beta$  (Fig. 3) is plotted over time. (Right) Probability distribution  $\rho(\beta)$  over the entire trajectory.



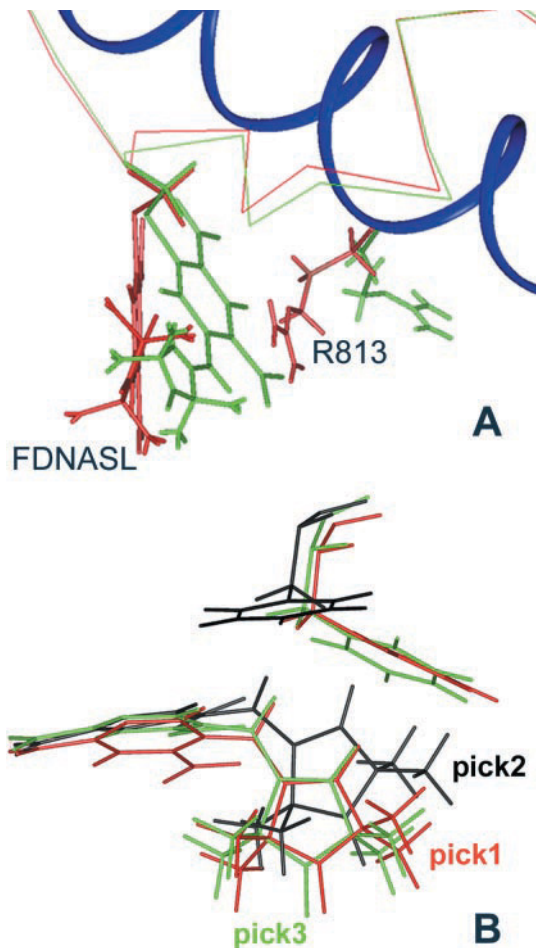


FIGURE 9 (A) Average D131C-FDNASL and Arg-813 conformers over the first 9 ns of the MD trajectory (red) and over last 5 ns of the trajectory (green). The heavy chain helix is shown as a blue ribbon. A different rotamer for Arg-813 produces a shift in the steric boundaries of the probe on a time scale of several nanoseconds. (B) Simulated annealing of A105C-FDNASL found three conformers—pick1, pick2, and pick3—representing local minima similar to within average probe RMS differences  $< 1.6$  Å (pick1-pick2 = 1.55, pick2-pick3 = 1.64, pick1-pick3 = 0.60)

entire spin label in the last 5 ns of the trajectory, while maintaining the bimodal rotations of the nitroxide ring. The two average spin label atom positions are shown in Fig. 9 A. The shift can also be seen in the trajectory (Fig. 8) as a sudden increase of  $\sim 0.5$  radians in the angle  $\beta$  at 9 ns. In the actual protein, these shifts probably occur as side chains exchange between different rotamers, partially blurring the distinct modes. This is apparent in the experimental EPR spectrum, which may display motional averaging.

#### M60C

Like D131C-FDNASL, the trajectory of the spin label attached to C60 displays bimodal dynamics but on a much faster timescale on the order of  $\sim 81$  ps (Fig. 8; Table 1). The spin label's partially exposed conformation on the RLC and fast bimodal time scale indicate that its nearby groups assume a conformation that lowers the energy barrier between rotameric states of the pyrrolidiny ring.

#### M72C

The spin label FDNASL bound to C72 shows fluctuating orientation and slow energy equilibration over the first 4 ns of this trajectory. During this equilibration period, the spin label appears to explore two orientations inside a crowded binding pocket. The spin label displays dynamics about only one of these orientations for the rest of the simulation, but the relatively high average potential energy suggests that there is a more stable global energy minimum that has not been reached.

#### M129C

This probe lies between the essential and regulatory light chains and is partially exposed. The MD displays single-mode dynamics but with a larger amplitude than at C108. A tryptophan residue (W21) in the essential light chain is the closest to the nitroxide group and has an average confor-

TABLE 1 Correlation times for trajectories were determined by fitting  $G(\tau)$  to exponential functions

	$\tau_{c1}$ (very fast) (ps)	$\tau_{c2}$ (fast) (ps)	$\tau_{c3}$ (slow) (ps)	$y_0$	Asymptote over $\tau = 1$ ns
C108	$0.70 \pm 0.01$	$24.9 \pm 0.06$	N/A	0.975	$\sim 0.98$
M129C	$1.22 \pm 0.007$	$63.7 \pm 0.3$	N/A	0.92	0.933
M60C	$0.492 \pm 0.004$	$65.21 \pm 0.15$	$81.7 \pm 0.04$	0.791	0.769
M72C	$1.13 \pm 0.013$	$16.17 \pm 0.019$	$113.5 \pm 0.14$	0.972	0.952
D131	$0.023 \pm 2.5e18$	$32.5 \pm 1.6$	$210.3 \pm 3.9$	0.56	0.61382
G95	$1.6 \pm 0.005$	$12.7 \pm 0.033$	N/A	0.84	0.877
A105	$0.23 \pm 1.22e-6$	$18.0 \pm 0.16$	$180.4 \pm 16.8$	0.99	0.99

$\tau_{c1}$  and  $\tau_{c2}$  were obtained by fitting over the first 50 ps to  $G(\tau) = y_1 \exp(-\tau/\tau_{c1}) + y_2 \exp(-\tau/\tau_{c2}) + y_0$ . The fits are good: asymptote values  $y_0$  in the  $\tau = 50$  ps window accurately reproduce autocorrelation equilibria over the entire autocorrelation window ( $\tau = 1$  ns) (the first 8 ns of the G95C trajectory were used for asymptote determination). For bimodal trajectories  $\tau_3$  was obtained by fitting  $G(\tau)$  to a single exponential over the first 1 ns, except for the G95C trajectory where the two modes exchange over a timeframe too long to be determined. The asymptote of this fit curve corresponded well to the autocorrelation equilibrium over  $\tau = 4$  ns.



mation showing a roughly planar configuration with the methyl groups on FDNASL.

### G95C

C95 is on the so-called “linker helix” of the RLC. Because of its sequence position on the helix, the spin label probably projects away from the protein. Fourteen nanoseconds of MD simulation show two modes of dynamics about different minima, each lasting  $\sim 9$  and 5 ns, respectively.

Given the limitations of our methods, the G95C model is most problematic because the spin label is highly exposed. In the MD simulation, the spin label appears to lie down on the surface of the protein, but this is poorly accounted for with an *in vacuo* model. Furthermore, such an exposed probe with few steric restrictions may have many possible conformations across a large region of conformational space with similar energies, only a few of which are revealed by 14 ns of dynamics simulation. Thus, a simulated annealing procedure was used to examine other possible minima.

#### *Simulated annealing of G95C-FDNASL*

Four different conformations of the spin probe were constructed by rotating the spin probe about the cysteine sulfur and methylene carbon and locally minimizing each. These structures were then used as starting conformers for MD trajectories for 200 ps at 600 K. The three lowest-energy frames from each 600 K trajectory were chosen for subsequent energy minimization and MD simulation for 6 ns at 300 K, yielding a total of 12 trajectories. The 12 trajectories with annealed starting structures had backbone average structures unwound from their native helices. Average potential energies across the annealed trajectories are  $\sim 940$  kcal/mol, whereas the original minimized structure produced a MD trajectory with an average potential energy of  $\sim 840$  kcal/mol. Because the original G95C-FDNASL trajectory had the lowest energy and average conformation most congruent with the crystal structure, we used this trajectory in our analysis (Fig. 8).

#### *A105C-FDNASL*

The A105C-FDNASL trajectory was computationally unstable because, apparently, the spin label and its crowded binding site were not adequately equilibrated. To remedy this, an annealing procedure was used. A 200-ps MD trajectory was simulated at 600 K, and the three lowest-energy conformations from 500 frames were chosen, called pick1, pick2, and pick3 (Fig. 9 B). All three conformations were minimized, resulting in average spin label RMS differences between the conformers of less than 1.6 Å. MD using each starting structure was simulated for 10 ns at 300 K, and each

produced a convergent trajectory about its local minimum. However, upon velocity perturbation at 6 ns in the pick2 trajectory, a rotameric shift of nearby phenylalanine residue F109 into a previously unseen conformation allowed the spin label-protein system to assume a lower-energy state by nearly  $-80$  kcal/mol for the rest of the simulation. Dynamics about this new local minimum was not only more stable, but had a calculated order parameter of 0.78, very close to the experimentally measured order parameter of 0.8. The order parameters of the pick1 and pick3 trajectories were  $\sim 0.34$  and  $\sim 0.25$ , respectively. This suggests that a realistic, stable minimum was found, and we use the last 4 ns of the pick2 trajectory as the representative structure for A105C-FDNASL.

In general, we note that of all the mutant structures simulated, the only MD trajectory that requires significant rearrangement of the side chains for equilibration appears to be A105C, due to the “buried” nature of the probe. In our convergence studies of C108, as in annealing of G95C, the lowest-energy dynamics are for models that perturb original protein structure the least. This is expected, because we know that the attachment of a spin label preserves functionality in the muscle fiber.

### Time scales of spin label motion

Autocorrelation (Eq. 3) was performed on all trajectories over the full 14-ns simulation, and all required multiexponential functions (i.e., multiple correlation times) to fit each correlation function, as expected for the persistent, quasi-harmonic motions present in a MD simulation. While correlated motions persist on many time scales, it is useful to characterize three types of motion: a “very fast” decay ( $\leq 1$  ps) reflecting the motion of the spin label atoms at 300 K; a “fast” motion when the spin label explores the conformations about a central dynamic mode ( $\sim 50$  ps), and in some cases, a “slow” motion when the spin label samples different modes (on the order of 500 ps). To determine “very fast” and “fast” time constants, an autocorrelation window of 50 ps was used to fit a biexponential function. To determine “slow” time constants for bimodal trajectories, an autocorrelation window of 1 ns was used to fit the single-exponential function of time constant  $\tau_{\text{slow}}$ . The resulting values are shown in Table 1.

The “fast” correlation times for all trajectories are near 50 ps, and the fast-motion limit can be safely assumed if EPR spectra were to be simulated from these MD trajectories. The “slow” rotational time constant for D131C-FDNASL is  $\sim 210$  ps. For the two modes present in the G95C-FDNASL trajectory, if in fact they are exchanging over time, the “slow” time constant would be even longer, on the time scale of nanoseconds; however, as the trajectory length is limited, we cannot say this with certainty. By comparing MD simulation with EPR studies of free spin labels, a previous study has estimated that the viscous effects of

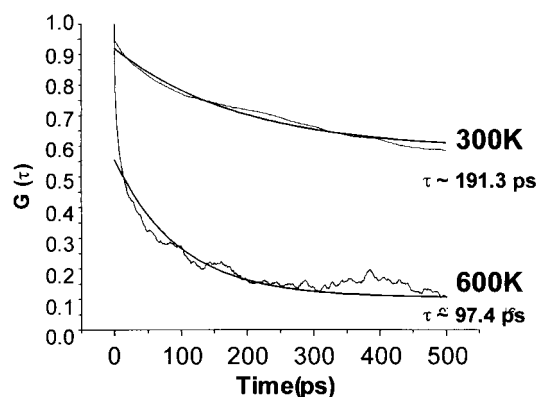


FIGURE 10 Autocorrelations of trajectory D131C at 300 and 600 K. Probe trajectory autocorrelations for D131C are only approximately exponential. Here first-order decays are fit over 500 ps of the trajectory as a function of temperature.

solvent increase  $\tau_c$  by roughly a factor of 3 (Steinhardt and Hubbell, 1996). If this is the case, the actual correlation time of the spin label for a bimodal trajectory may be well into the 10-ns range, a time scale in which fast motional averaging of EPR tensors cannot be assumed. This has broad implications for resolving the potentially ambiguous line-shapes attributable to time scale and orientational disorder in an EPR spectrum. In EPR spectroscopy, one often makes conclusions based on the assumption that a spin label undergoes fast diffusion within a restricted cone of motion. In some cases, bimodal exchange may be a better model, and a detailed MD model would be an indispensable tool to help resolve this. Also, by explicitly computing the autocorrelation directly from a trajectory, it is possible to formulate more precise simulations of EPR spectra from first principles.

Fig. 10 shows the autocorrelation of 500 ps of the D131C-FDNASL trajectory simulated at 300 and 600 K. The autocorrelation of the first 50 ps was also done (not shown), with  $t = 14.3$  ps at 300 K and  $t = 8.0$  ps at 600 K. The differences in single-exponential fits across different time windows ( $\tau = 50$  ps and  $\tau = 500$  ps) show the persistence of correlated motion with increasing time scale. In both time windows, the 600-K trajectories have rotational time constants approximately one-half those of the 300-K trajectory, confirming the temperature-dependent Debye relationship  $\tau_c \sim \eta V/kT$ . From the asymptote of each autocorrelation, we can discern that the 600-K trajectory, as expected, is much more disordered. This demonstrates the difficulty in simply increasing temperature in an attempt to allow the spin label to explore more conformational space and thus better characterize its motion. Whereas we can extrapolate the expected time constant of motion at a given temperature from the Debye relation, at high temperature the conformational space available to the probe and surrounding protein is unrealistically large, and therefore

not necessarily relevant to the actual dynamics at ambient temperature.

### Comparison of experimental and simulated order parameters

The order parameters calculated from both EPR spectra and MD trajectories are shown in Fig. 11. Error bars in the simulated values are the standard deviation of order parameters for 1-ns segments of the longer 14-ns trajectory. (In the case of the A105C-FDNASL, the trajectory is 10 ns long.) The order parameters of most spin-labeled mutants are excellently predicted to within 0.05, with the exception of the more exposed spin labels D131C-FDNASL and G95C-FDNASL, for which molecular dynamics trajectories predict lower order parameters than measured.

It is clear from the comparison that our molecular dynamics procedure provides an excellent way to perform “virtual” mutagenesis to predict spin-labeled mutants that have a high measured order parameter. Such mutants could later be expressed and used as useful experimental tools to detect the rotational motion and orientation of the proteins to which they are attached. Furthermore, by having a molecular model of the spin label dynamics at a given labeling site, it is possible to resolve EPR spectra with unprecedented detail, as the molecular dynamics trajectory contains quantitative information about orientation, amplitude, and time scale of motion, whereas most SDSL studies are necessarily qualitative.

Why do G95C-FDNASL and D131C-FDNASL predict lower order parameters? The first, most obvious, reason for this is the way order parameter is calculated from our trajectories. All order parameters are calculated with respect to the most populous mode, even for trajectories with multiple modes. Thus, the spin label’s sampling of multiple minima contributes a large amount of disorder when calculated with respect to the major mode. However, because the sampling of these modes occurs on a slow time scale, the EPR spectrum is less sensitive to the motional averaging across the multiple modes, yielding a higher “apparent” order parameter. For example, consider the two dynamical modes present in the G95C-FDNASL trajectory. Each mode is stable on a time scale of several nanoseconds or perhaps longer, since the modes persist longer than can be completely characterized in the length of the simulation. The observed barrier crossing from one minimum to another is induced by a velocity perturbation. From this, we can assume that diffusion between these two modes in the simulation proceeds in the slow limit, and in this limiting case, the EPR spectrum should be a linear combination of the spectra for each mode. Because the length of the simulation does not adequately characterize the time spent around each observed minima, we are unable to determine the ratio of these components. However, an “apparent” order parameter measured from the EPR spectrum would report the highest-

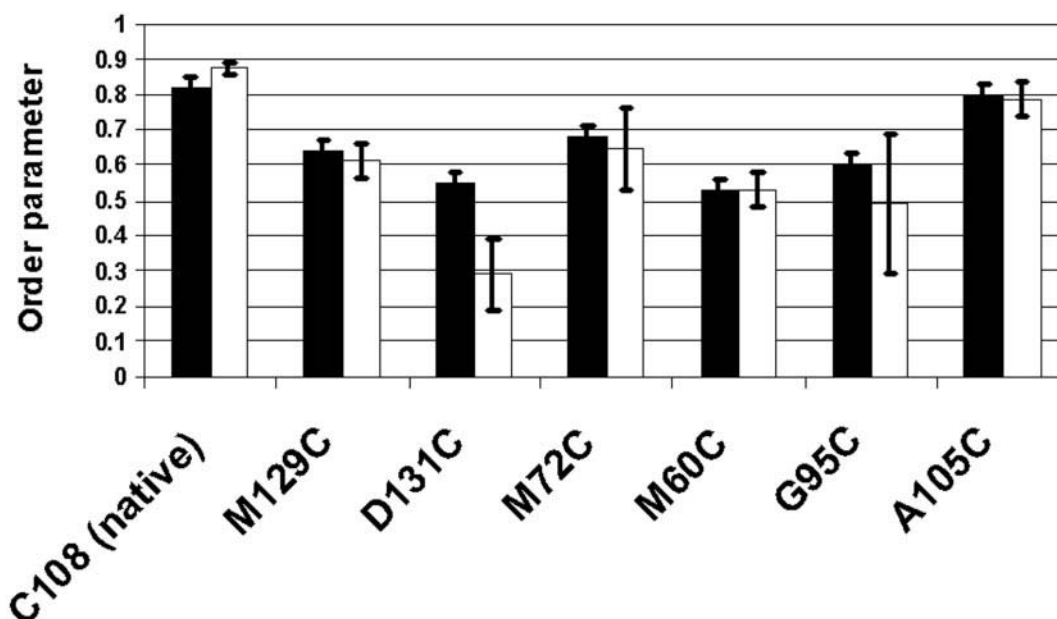


FIGURE 11 Experimental (black) order parameters of spin-labeled mutants determined by EPR spectroscopy, plotted against simulated (white) order parameters calculated directly from molecular dynamics trajectories. Error bars in the simulated values are the standard deviation of order parameters across 1-ns segments. For A105C, three trajectories were simulated, but only the order parameter for the dynamics trajectory about the lowest-energy minimum is shown.

order mode, as reflected in the largest tensor splittings. Indeed, whereas the second mode in the trajectory has an order parameter of  $\sim 0.37$ , the calculated order parameter across the first 9 ns of the trajectory, which includes only the first mode, is 0.62, very close to the value of 0.60 measured from the experimental EPR spectrum.

In the case of D131C-FDNASL, the bimodal dynamics observed in the simulation explains the discrepancy between simulated and experimental order parameter. Each of the dynamical modes in the trajectory, when fit to multiple Gaussians and analyzed individually, have high order parameters (0.74, 0.87, 0.91, and 0.94), whereas the overall order parameter calculated with respect to the most populous mode has an order parameter of 0.28. The apparent order parameter of the experimental spectrum is 0.55. This, together with a molecular dynamics trajectory that displays bimodal fluctuations on a timescale of several hundred picoseconds, suggests that motional averaging on an intermediate time scale is occurring to produce the observed EPR spectrum for D131C-FDNASL.

Another reason for disagreement between the MD simulation and experiment may be from the exclusion of solvent from the molecular dynamics model. Our initial attempts at simulating with explicit water were unsuccessful because the computational limits of the large model confined trajectory lengths to only several picoseconds. However, inclusion of solvent may only have subtle effects. There is evidence to suggest that the greatest contribution of solvent would be to simply increase the rotational time constant of

the probe due to viscous damping, with other effects being much more subtle, and perhaps negligible. Columbus et al. (2001) note that the energy barriers separating solvent-exposed rotamers of the nitroxide ring of spin labels attached to T4-lysozyme can be accounted for solely by the viscous effects of solvent and not interactions affecting internal energies. Steinhoff and Hubbell (1996) have speculated that with the addition of solvent, the hydrophobic effect would increase, whereas at the same time the van der Waals attraction would decrease, partially canceling each others' effects. Future molecular dynamics studies that incorporate an implicit solvent model will help further elucidate the effect of solvent on probe dynamics. The good agreement of predicted and experimental order parameters using an *in vacuo* model in this study suggest that it is reasonable to neglect solvent except in cases where the spin label is thoroughly exposed, as in the G95C model. Exposed mutants generally have low order parameters, and because our original aim of this project was to find "virtual mutants" with high order parameter, we have seen that it is possible to neglect solvent without catastrophic consequences.

### Side chain interactions with the spin label

We know that because of surrounding residues, spin labels exhibit anisotropic dynamics. Yet SDSL is generally thought to report local structure and dynamics in an unbiased manner. Is it possible that the order parameter pre-

dicted by our MD simulation simply reflects the general topology of the site where the spin label binds, and therefore we could use local topology alone to predict good sites for binding? For each mutant trajectory, we plotted predicted order parameter versus the density of atoms within 5 Å of the spin label. There is poor correlation between the two quantities, suggesting that spin label dynamics is a more complicated story.

Do specific chemical residues near the spin label affect its dynamics? We calculated the average RMS distances and relative diffusion constants between spin label atom groups and the eight closest residues in each mutant model, but the results of these calculations showed no clear correlation with order parameter. It was observed that in the two trajectories with the highest predicted order parameter (C108 and A105C) F109 is the closest residue, but this evidence is circumstantial. Overall, we see that spin label dynamics are sufficiently complex to necessitate MD simulation.

### Absolute orientation of the FDNASL in muscle fibers

Changes in the orientation of spin-labeled RLC of  $\sim 36^\circ$  with respect to the actin axis have been observed by detecting the orientational anisotropy of attached spin probes in the muscle fiber by EPR spectroscopy (Baker et al., 1998). These data suggest that when a muscle fiber is in rigor (myosin strongly bound to actin), the light chain domain is predominantly at a single orientation relative to the actin filament in oriented muscle fibers. This observation provides another opportunity to compare experimental results with our computer model of FDNASL attached at position 108 of the RLC. Using the published coordinates of an actin filament decorated with chicken skeletal myosin fragments (Mendelson and Morris, 1997), we oriented our model of the light chain domain with respect to the actin filament. This alignment oriented our structure in the muscle fiber reference frame, allowing us to calculate  $\theta$ , the angle of the nitroxide  $z$  axis with respect to the actin filament. The aligned model structure reported a value of  $\theta = 42^\circ$  whereas the experimentally determined rigor value determined by EPR was  $\theta = 38^\circ \pm 4^\circ$ . This is remarkable agreement, considering several assumptions were made in the alignment model (the decorated filament model itself was from another species, the chicken gizzard light chain was homology modeled onto the scallop light chain structure, and the crystal structure probably does not reflect the inherent flexibility of the light chain domain (Nyitrai et al., 2000; Ramachandran and Thomas, 1999; Roopnarine et al., 1998; Volkmann et al., 2000)).

## CONCLUSION

The order parameters calculated from MD trajectories of site-directed spin labels agree well with those determined by EPR spectroscopy, even though visual inspection of the structures surrounding these labeling sites does not provide enough information to predict probe mobilities. Thus, our procedure provides an effective way to perform "virtual" mutagenesis to predict spin-labeled residues that will display desired mobility. This can reduce the time required to synthesize, express, and assess the usefulness of constructed mutants.

MD simulation is useful as a tool to supplement EPR spectroscopy. Amplitudes of spin label motion, rotational time scales, angular distribution, and absolute orientation can be extracted from a dynamics trajectory and used to resolve ambiguous or indeterminate spectra, particularly those that may result from bimodal or multimodal dynamics. As the quality of future MD simulations improves, future studies will involve simulating accurate EPR spectra directly from molecular dynamics trajectories of spin probes, a prospect that offers a new level of detail to complement SDSL studies.

We thank Adam Butensky-Bartlett, Claire Chisolm, Will Meland, and Greg Wilde, who made significant contributions to the development of this project. We also thank Octavian Cornea for help in preparation of the manuscript.

This work was supported by grants from the National Institutes of Health Grant AR32961-16, the Muscular Dystrophy Association, and the Minnesota Supercomputer Institute (to D.D.T.). L.E.W.L. was supported by a National Institutes of Health training grant and by a Doctoral Dissertation Fellowship from the University of Minnesota Graduate School.

## REFERENCES

- Allen, M. P., and D. J. Tildesley. 1987. *Computer Simulation of Liquids*. Oxford University Press, Inc., New York.
- Baker, J. E., I. Brust-Mascher, S. Ramachandran, L. E. LaConte, and D. D. Thomas. 1998. A large and distinct rotation of the myosin light chain domain occurs upon muscle contraction. *Proc. Natl. Acad. Sci. U. S. A.* 95:2944–2949.
- Brust-Mascher, I., L. E. LaConte, J. E. Baker, and D. D. Thomas. 1999. Myosin light-chain domain rotates upon muscle activation but not ATP hydrolysis. *Biochemistry* 38:12607–12613.
- Columbus, L., T. Kalai, J. Jeko, K. Hideg, and W. L. Hubbell. 2001. Molecular motion of spin-labeled side chains in alpha-helices: analysis by variation of side chain structure. *Biochemistry* 40:3828–3846.
- Dauber-Osguthorpe, P., V. A. Roberts, D. J. Osguthorpe, J. Wolff, M. Genest, and A. T. Hagler. 1988. Structure and energetics of ligand binding to proteins: *Escherichia coli* dihydrofolate reductase-trimethoprim, a drug-receptor system. *Proteins* 4:31–47.
- Dewar, M. J. S., E. G. Zoebisch, E. F. Healy, and J. J. P. Stewart. 1985. AM1: a new general purpose quantum mechanical model. *J. Am. Chem. Soc.* 107:3902–3909.
- Freed, J. H. 1976. *Spin Labeling: Theory and Applications*. L.J. Berliner, editor. Academic Press, New York. 53–132.
- Gaffney, B. J. 1976. Practical consideration for the calculation of order parameters for fatty acid or phospholipid spin labels in membranes. *In*



- Spin Labeling: Theory and Application. LJ Berliner, editor. Academic Press, New York. 567–571.
- Houdusse, A., and C. Cohen. 1996. Structure of the regulatory domain of scallop myosin at 2 Å resolution: implications for regulation. *Structure*. 4:21–32.
- Hubbell, W. L., and C. Altenbach. 1994. Investigation of structure and dynamics in membrane proteins using site-directed spin labeling. *Curr. Opin. Struct. Biol.* 4:566–573.
- Hubbell, W. L., A. Gross, R. Langen, and M. A. Lietzow. 1998. Recent advances in site-directed spin labeling of proteins. *Curr. Opin. Struct. Biol.* 8:649–656.
- Hubbell, W. L., H. S. McHaourab, C. Altenbach, and M. A. Lietzow. 1996. Watching proteins move using site-directed spin labeling. *Structure*. 4:779–783.
- Langen, R., K. J. Oh, D. Cascio, and W. L. Hubbell. 2000. Crystal structures of spin-labeled T4 lysozyme mutants: implications for the interpretation of EPR spectra in terms of structure. *Biochemistry*. 39: 8396–8405.
- Maita, T., J. I. Chen, and G. Matsuda. 1981. Amino-acid sequence of the 20,000-molecular-weight light chain of chicken gizzard-muscle myosin. *Eur. J. Biochem.* 111:417–424.
- Maita, T., K. Konno, T. Ojima, and G. Matsuda. 1984. Amino acid sequences of the regulatory light chains of striated adductor muscle myosins from Ezo giant scallop and Akazara scallop. *J. Biochem. (Tokyo)*. 95:167–177.
- Mendelson, R., and E. P. Morris. 1997. The structure of the acto-myosin subfragment 1 complex: results of searches using data from electron microscopy and x-ray crystallography. *Proc. Natl. Acad. Sci. U. S. A.* 94:8533–8538.
- Nyitrai, M., G. Hild, A. Lukacs, E. Bodis, and B. Somogyi. 2000. Conformational distributions and proximity relationships in the rigor complex of actin and myosin subfragment-1. *J. Biol. Chem.* 275:2404–2409.
- Ostap, E. M., H. D. White, and D. D. Thomas. 1993. Transient detection of spin-labeled myosin subfragment 1 conformational states during ATP hydrolysis. *Biochemistry*. 32:6712–6720.
- Persechini, A., and D. J. Hartshorne. 1983. Ordered phosphorylation of the two 20,000 molecular weight light chains of smooth muscle myosin. *Biochemistry*. 22:470–476.
- Ramachandran, S., and D. D. Thomas. 1999. Rotational dynamics of the regulatory light chain in scallop muscle detected by time-resolved phosphorescence anisotropy. *Biochemistry*. 38:9097–9104.
- Robinson, B. H., L. J. Slutsky, and F. P. Auteri. 1992. Direct simulation of continuous wave electron paramagnetic resonance spectra from Brownian dynamics trajectories. *J. Chem. Phys.* 96:2609–2616.
- Roopnarine, O., A. G. Szent-Gyorgyi, and D. D. Thomas. 1998. Microsecond rotational dynamics of spin-labeled myosin regulatory light chain induced by relaxation and contraction of scallop muscle. *Biochemistry*. 37:14428–14436.
- Squier, T. C., and D. D. Thomas. 1989. Selective detection of the rotational dynamics of the protein-associated lipid hydrocarbon chains in sarcoplasmic reticulum membranes. *Biophys. J.* 56:735–748.
- Steinhoff, H. J., and W. L. Hubbell. 1996. Calculation of electron paramagnetic resonance spectra from Brownian dynamics trajectories: application to nitroxide side chains in proteins. *Biophys. J.* 71:2201–2212.
- Thomas, D. D., and R. Cooke. 1980. Orientation of spin-labeled myosin heads in glycerinated muscle fibers. *Biophys. J.* 32:891–906.
- Tinoco, I., K. Sauer, and J. C. Wang. 1985. Physical Chemistry. Prentice-Hall, Inc., Englewood Cliffs, NJ.
- Volkman, N., D. Hanein, G. Ouyang, K. M. Trybus, D. J. DeRosier, and S. Lowey. 2000. Evidence for cleft closure in actomyosin upon ADP release. *Nat. Struct. Biol.* 7:1147–1155.
- Xie, X., D. H. Harrison, I. Schlichting, R. M. Sweet, V. N. Kalabokis, A. G. Szent-Gyorgyi, and C. Cohen. 1994. Structure of the regulatory domain of scallop myosin at 2.8 Å resolution. *Nature*. 368:306–312.